ISET Journal of Earthquake Technology, Paper No. 586, Vol. 61, No. 2, June 2024, pp. 41-53

SEISMIC HAZARD MAPPING FOR PEAK GROUND VELOCITY – II: NATIONAL CAPITAL REGION, INDIA

V.W. Lee
Dept. of Civil Engineering, Univ. of Southern California
Los Angeles, CA, 90089, USA, E mail id: *vlee@usc.edu*

M.D. Trifunac
Dept. of Civil Engineering, Univ. of Southern California
Los Angeles, CA, 90089, USA, E mail id: *misha.trifunac@gmail.com*

I.D. Gupta (Corresponding Author)
Independent Scholar, Row House 4, Suncity
Pune 411051, India, E mail *id: idgrh4@gmail.com*

ABSTRACT

We present the probabilistic seismic hazard maps for $V_{\max}$, peak velocity of strong earthquake ground motion in National Capital Region (NCR) of India. The maps are presented for all possible combinations of geological site parameters s (sediments, intermediate sites, basement rock sites) and soil site parameters s_L ("rock soil", stiff soil and deep soil). The user will select the s and s_L parameters based on the local site investigation. These maps can be utilized to evaluate (a) the strains near ground surface during strong earthquake ground motion, (b) the areas where buildings may be damaged during future strong ground motion, and (c) how $V_{\max}$ can be utilized to obtain the estimates of pseudo-static forces in ground level columns of long structures from the probabilistic estimates of relative displacement response spectra.

KEYWORDS: Probabilistic Maps of $V_{\max}$; Peak Ground Strains; Differential Ground Motion; Pseudo Static Forces in Ground Floor Columns

INTRODUCTION

Traditional scaling of seismic ground motion for response analysis of engineering structures in terms of standard spectral shapes anchored to peak ground acceleration is not suitable for all engineering applications. For example, estimation of the maximum pseudo-static forces in long structures due to differential ground motion, estimation of peak strains near ground surface, or simplified criteria for damage of structures are required to be scaled by peak velocity of strong ground motion.

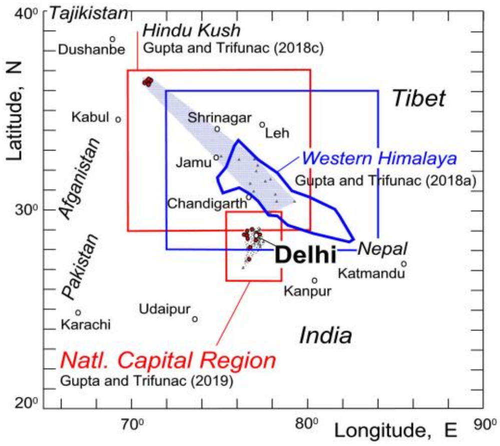

Fig. 1 Earthquake source areas along the Himalayan orogenic belt: North Western Himalaya (NWH), Hindu Kush Subduction (HKS), and the National Capital Region (NCR) (Gupta and Trifunac, 2017, 2018a, b, c, 2019), with seismic sources which contribute to the shaking hazard in NCR (modified from Lee et al. 2023)

The National Capital Region (NCR) is exposed to seismic hazard due to earthquakes in the North Western Himalaya (NWH) and the Hindu Kush Subduction (HKS) sources, in addition to local earthquakes in close proximity (Figures 1, 2). These three different seismic sources, which contribute to the seismic hazard in NCR are characterized by separate path-dependent attenuations of peak ground velocities V_{max} (Gupta and Trifunac 2023).

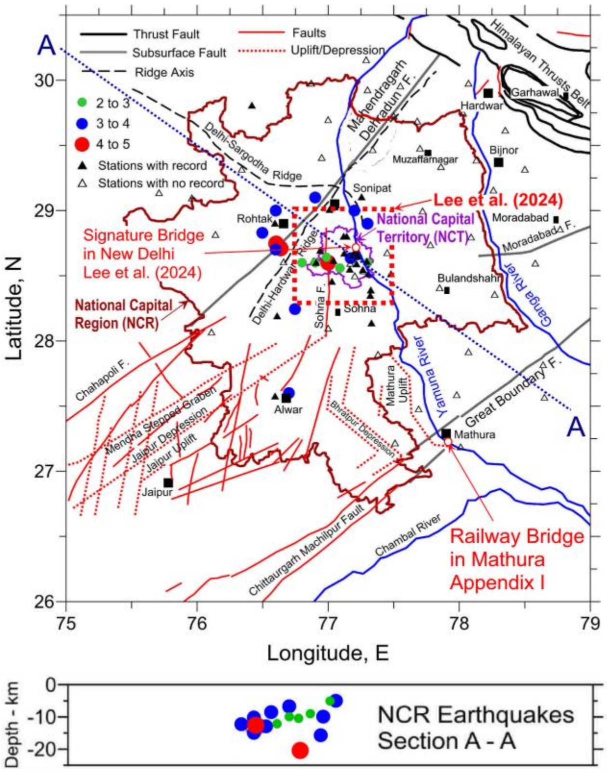

Fig. 2a (Top): Strong motion accelerograph stations (triangles) located in the NCR that recorded strong motion accelerations used to develop the attenuation equation for V_{max} due to local events in the area (Gupta and Trifunac 2023). Local earthquakes are shown with solid color circles with diameter proportional to magnitude. City of Mathura, the site of the Railway bridge over Yamuna River (Appendix I) is shown in the bottom right segmant of the figure. (Bottom): Projection of earthquake foci onto the vertical surface of Section A–A

In this paper we present seismic hazard maps of V_{max} for NCR of India (Figure 1 and 2), and illustrate through several examples their applications in engineering design along with the seismic hazard maps for Uniform Hazard Spectra of Pseudo Spectral Velocity (PSV) of strong motion (Gupta and Trifunac 2019). To avoid duplication, we refer the readers to our earlier paper on seismic microzonnation for V_{max} in Delhi (Paper I) (Lee et al 2023) for details.

SITE PROPERTIES, STRONG MOTION DATA AND METHODS OF ANALYSES

Computation of seismic hazard maps requires preparation of a comprehensive database on spatial distribution of seismic activity rates surrounding the site (Gupta et al 2022a), availability of ground motion scaling (attenuation) relations (see Appendix A in Paper I), and a method for probabilistic integration of the contributions from all the earthquake expected to occur in all the source zones affecting the site during an exposure period of Y years (see Appendix B in Paper I). In Paper I the geological site parameter s (Trifunac 2016; Trifunac and Brady 1975) was used in calculations of spatial distribution of hazard amplitudes for each site based on the available geological maps. This is practical to define it on the scale involving cities and even large metropolitan areas (Gupta et al. 2022a), but would result in too complex and rapid spatial variations on the scale required for mapping the hazard of large regions such as the NCR. Hence, in this paper we assume that the geological site parameter s at the site will be specified by the user from the available data on site geology. Likewise, the local soil site parameters generally also vary rapidly from point to point, making it impractical to prepare their detailed spatial maps for a large area, and hence it is proposed to be estimated for each site via site specific investigations during site preparation for construction. Therefore, in this paper we adopt the approach we used previously (Lee and Trifunac 2018; Gupta et al; 2022b) where we presented hazard maps for all nine combinations of s and s_L with s = 0, 1 or 2 and s_L = 0, 1 or 2. But in this paper, we illustrate the results for s = 0, 1 and 2 and for s_L = 1 only. Once the site parameters are determined for a construction site, the user can just select the appropriate map for a combination of s and s_L parameters and then just read the value of $V_{\max}$ at the desired latitude and longitude.

RESULTS

Figures 3a through 3c show the hazard maps of $V_{\max}$ in the NCR with contours of the $\log_{10}(V_{\max})$ amplitudes for exposure period $Y = 50$ years, at geological site conditions (sediments, $s = 0$; intermediate geological sites, $s = 1$, and basement rock sites $s = 2$), all on stiff soil type of site condition ($s_L = 1$), and for probabilities of exceeding at least once equal to 1%, 2%, 5% and 10%. It may be seen that, for sites on stiff soil (s_L = 1) and exposure period of 50 years, the peak ground velocity within the NCR area $V_{\max}$ is seen to increase from south to north, between 4 cm/s (for P = 10%) and 32 cm/s (for P = 1%).

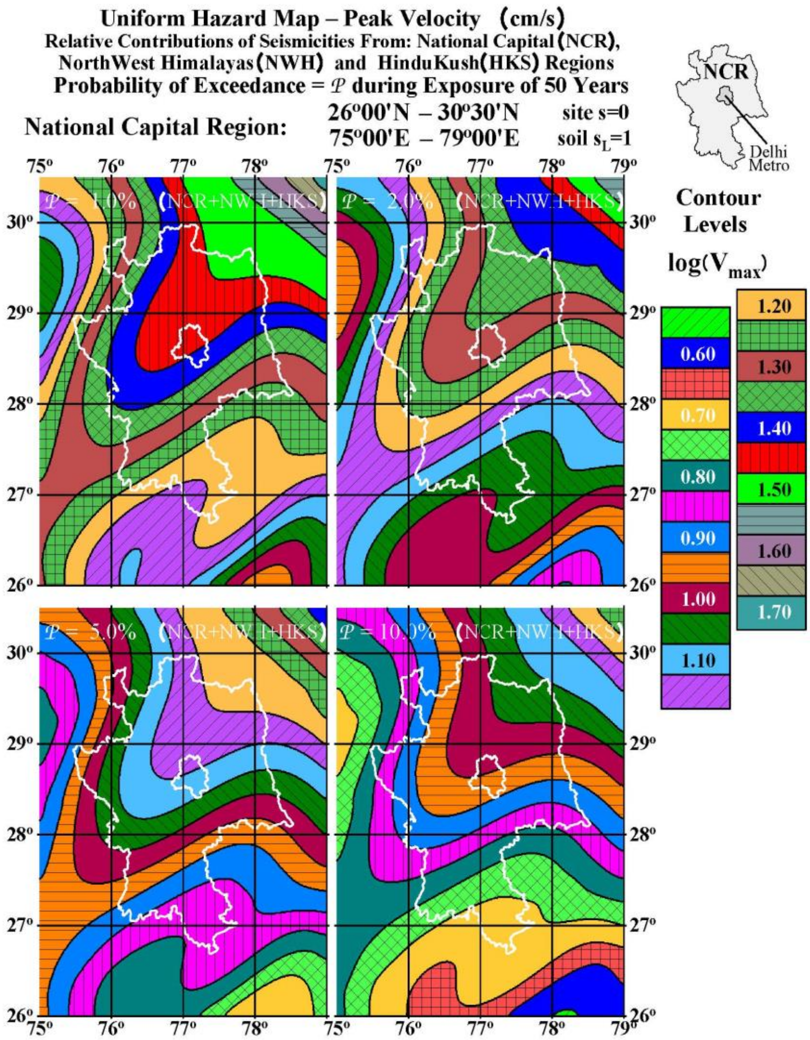

Fig. 3a Seismic Hazard map of NCR showing contours of $\log_{10}(V_{\max})$ in cm/s, for exposure period $Y = 50$ yrs, probabilities of exceedance $P = 1\%, 2\%, 5\%$ and 10%, for sites on sediments (s=0) and on stiff soil (s_L=1)

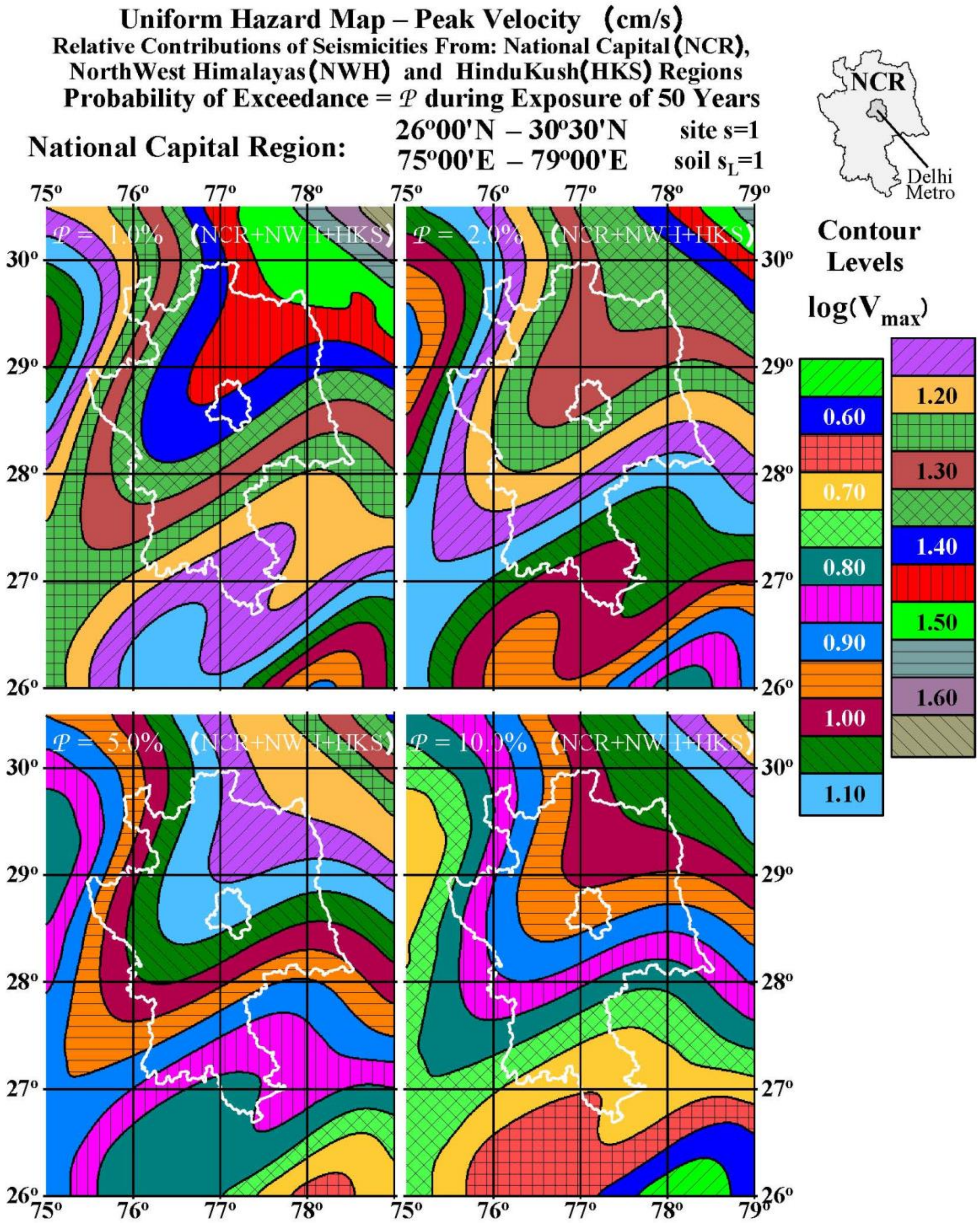

Fig. 3b Seismic Hazard map of NCR showing contours of $\log_{10}(V_{max})$ in cm/s, for exposure period $Y = 50$ yrs, probabilities of exceedance $P = 1\%, 2\%, 5\%$ and 10%, for sites on intermediate geological sites (s=1) and on stiff soil (s_L=1)

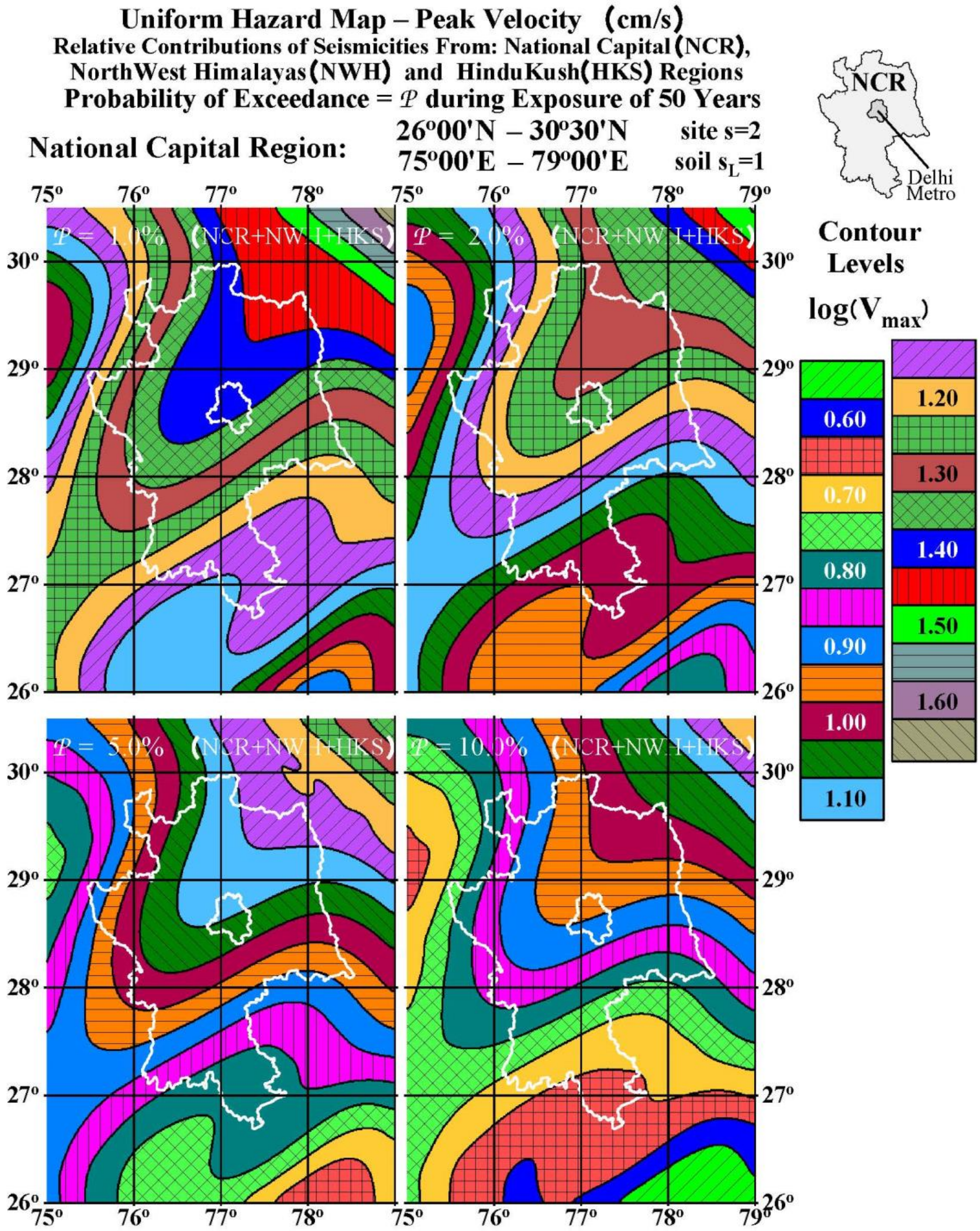

Fig. 3c Seismic Hazard map of NCR showing contours of $\log_{10}(V_{\max})$ in cm/s, for exposure period $Y = 50$ yrs, probabilities of exceedance $P = 1\%, 2\%, 5\%$ and 10%, for sites on basement geological sites (s=2) and on stiff soil (s_L=1)

Figures 3d through 3f show relative contributions to earthquake hazard maps of $V_{\max}$ in NCR. Contours are shown for the $\log_{10}(V_{\max})$ amplitudes, for exposure period Y=50 years, at three geological sites s = 0, 1 and 2, for soil site s_L = 1, and for probabilities of exceeding at least once equal to 10%. In each of the figures, there are three parts, with the top left part sowing contours based only on seismicity from earthquakes occurring in NCR. The bottom left part shows contours for contributions from earthquakes in NCR and NWH. The large segment on the right shows results for contributions from all three source regions: NCR, NWH and HKS. It is seen that the principal contribution to the hazard maps of $V_{\max}$ comes from NWH.

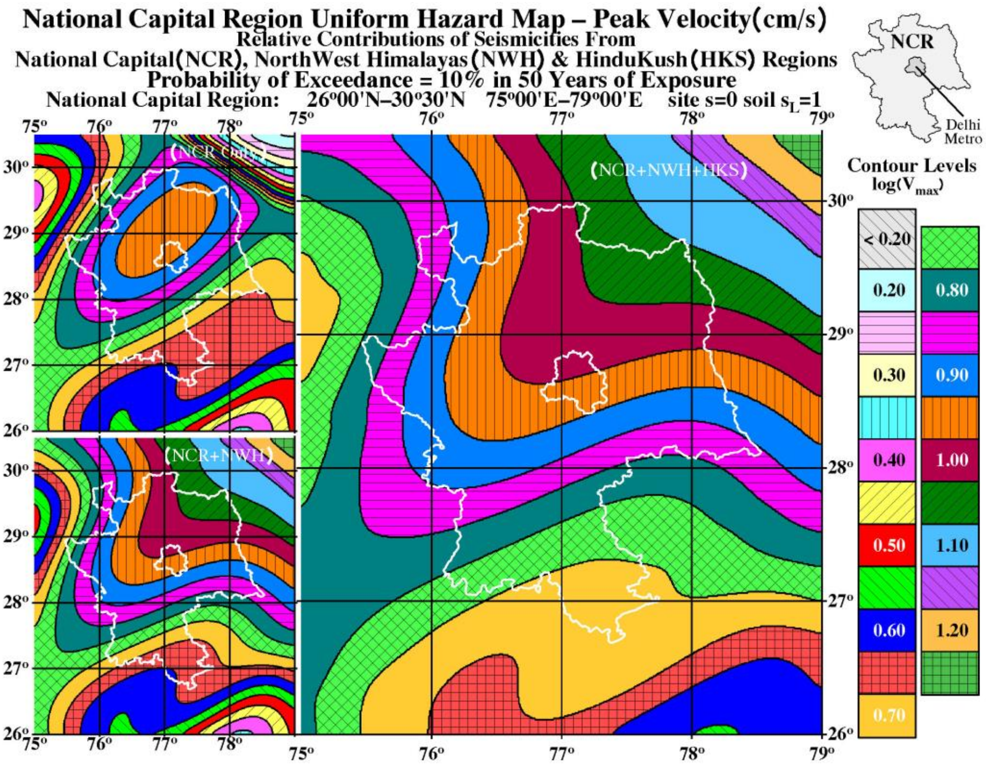

Fig. 3d Seismic hazard map of NCR: $\log_{10}(V_{\max})$ contours in cm/s, for exposure period Y = 50 yrs and probability of exceedance P = 10%, for sites on $s=0$ and $s_L=1$. Top left frame shows contribution from NCR only. Bottom left from NCR and NWH. Large frame on the right shows contribution from all three source zones NCR, NWH and HKS

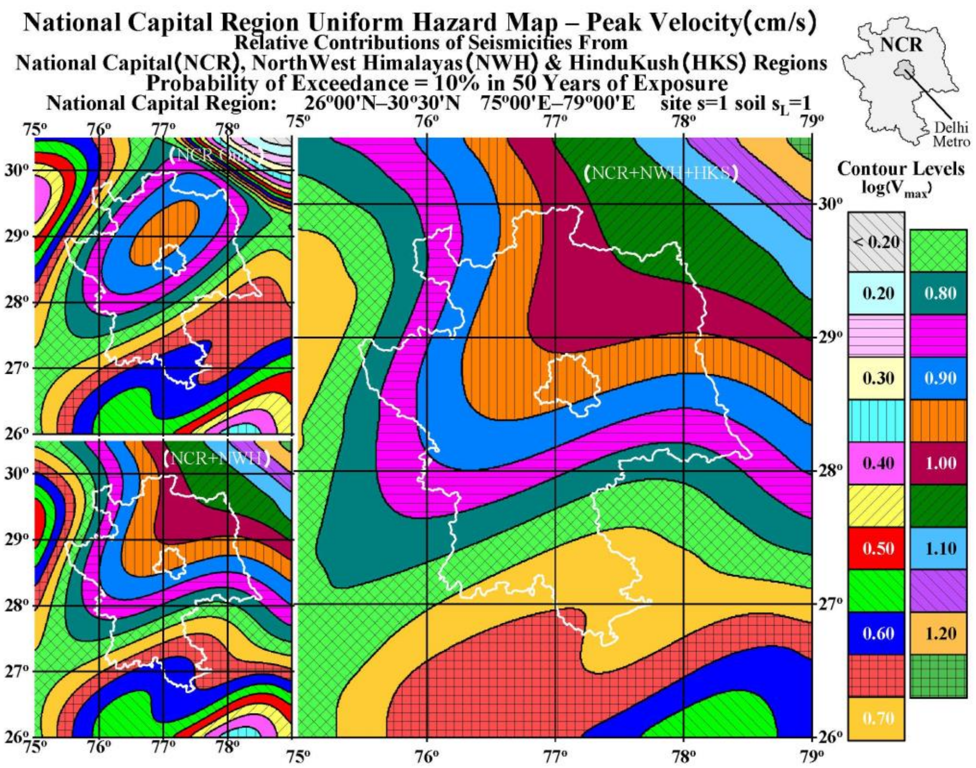

Fig. 3e Seismic hazard map of NCR: $\log_{10}(V_{\max})$ contours in cm/s, for exposure period Y = 50 yrs and probability of exceedance P = 10%, for sites on $s=0$ and $s_L=1$. Top left frame shows contribution from NCR only. Bottom left from NCR and NWH. Large frame on the right shows contribution from all three source zones NCR, NWH and HKS

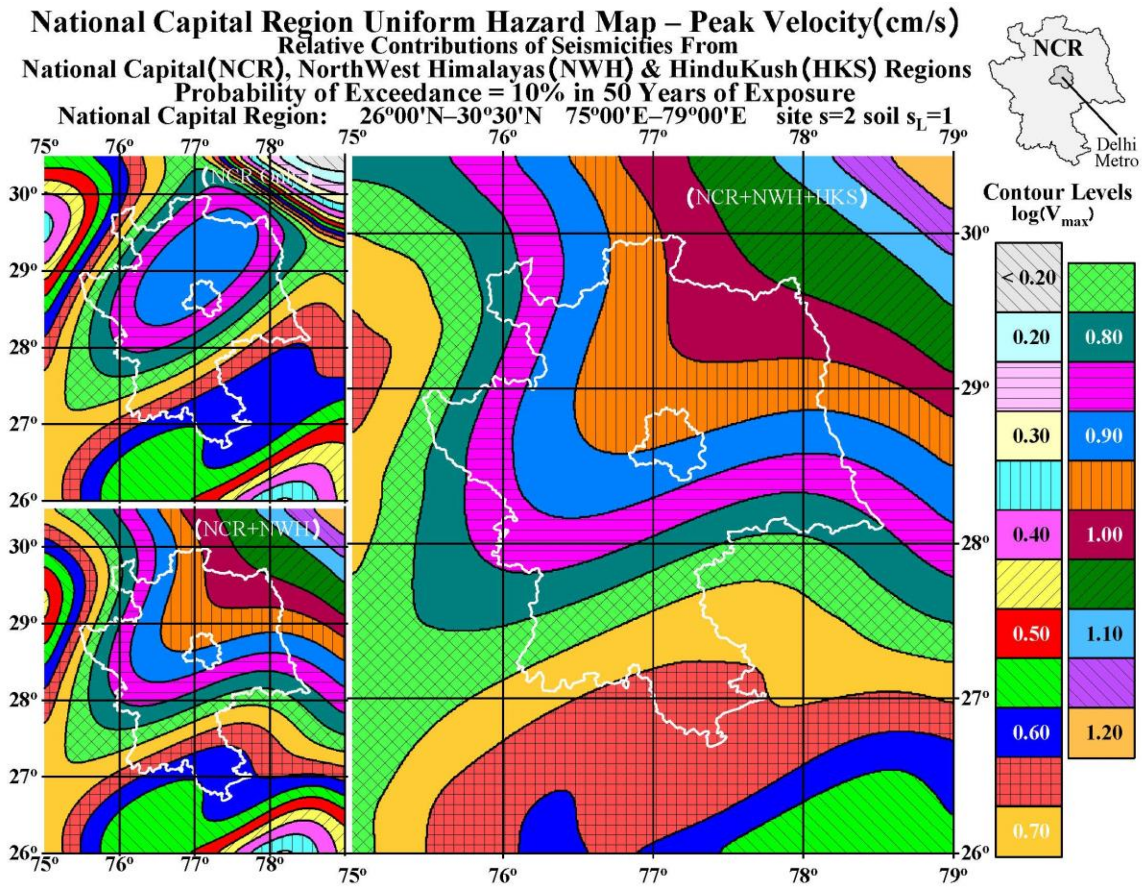

Fig. 3f Seismic hazard map of NCR: $\log_{10}(V_{\max})$ contours in cm/s, for exposure period Y = 50 yrs and probability of exceedance P = 10%, for sites on $s = 0$ and $s_L = 1$. Top left frame shows contribution from NCR only. Bottom left from NCR and NWH. Large frame on the right shows contribution from all three source zones NCR, NWH and HKS

Figure 4a and 4b show the ratios of the contributions to V_{max} from all the three seismic sources (NCR+NWH+HKS) and the contributions from (NWH+NCR) relative to NCR, respectively. It is seen that the ratios are in the range from 1.00 to 12.0 with values larger than 1.20 occurring outside NCR area in the upper right corner of the region. This is due to the contributions from seismic events in Northwest Himalayas. In the western and south-western part of NCR, comparing Figure 4a with Figure 4b illustrates how the contribution from distant HKS earthquakes becomes more significant only when the local seismicity is very low (Figure 2).

As in our paper about V_{max} in the Delhi Metro area (Lee et al. 2023), all results shown here are computed for the horizontal components of V_{max}. Since the scaling equations for V_{max} (Gupta and Trifunac 2023) are in terms of the logarithm of V_{max}, to convert all results to the vertical components of V_{max}, it is necessary to add –0.280 to $\log_{10}(V_{\max})$. That means, on linear scale the amplitudes of vertical components of V_{max} are 0.525 times those for the horizontal components of V_{max} .

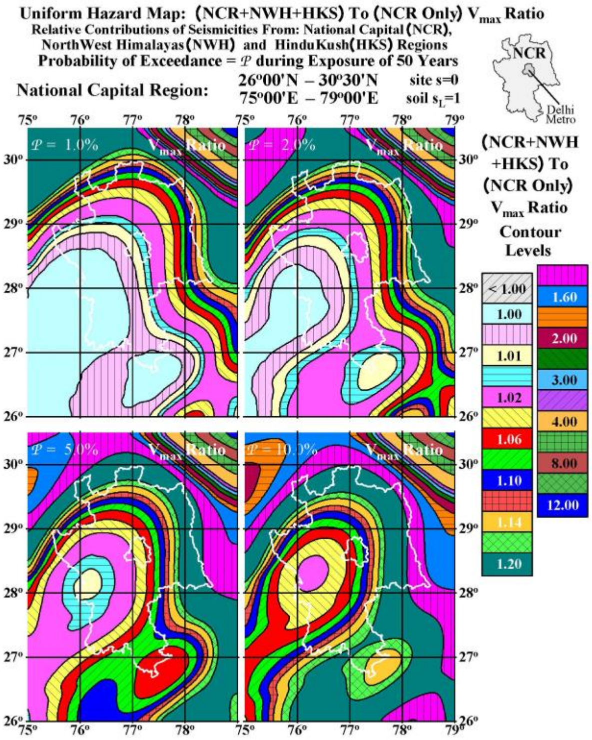

Fig. 4a Ratios of contributions to seismic hazard maps of V_{max} from (NCR+NWH+HKS) to (NCR only) for probabilities of exceedance $P = 1,\ 2,\ 5,\ 10\%$

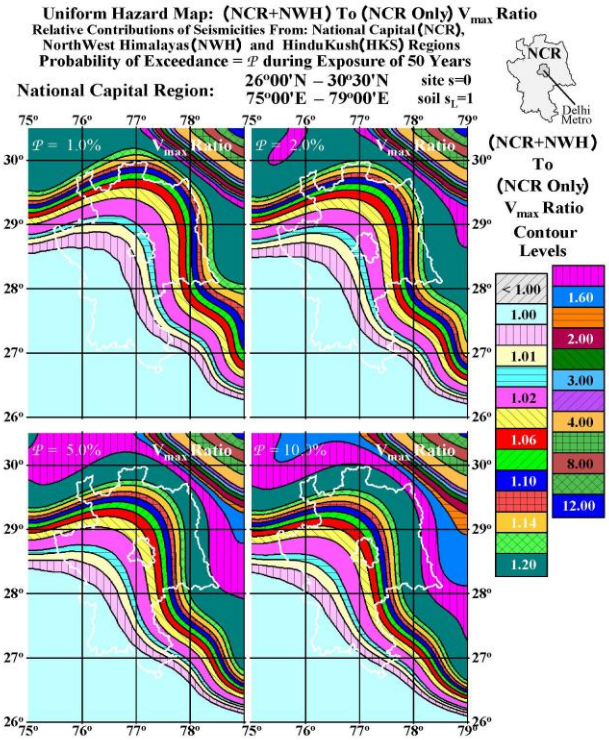

Fig. 4b Ratios of contributions to seismic hazard maps of V_{max} from (NCR+NWH) to (NCR Only) for probabilities of exceedance $P = 1,\ 2,\ 5,\ 10\%$

EXAMPLES OF PRACTICAL USES OF V_{max}

Maximum Strains in the Soil Near Ground Surface

The strain in the soil accompanying strong ground motion can be approximated by V_{max}/β, where β is the near surface shear wave velocity in the ground (Todrovska and Trifunac, 1996a,b). As in the Paper I, this has been illustrated for NCR for an assumed uniform $\beta = 100\, m/s$ over the complete area. The result is shown in Figure 5, which is a scaled down version of Figure 3a, by using a dividing factor of $\beta = 100\, m/s$ or $10^4\, cm/s$. When desired values of β are different from $100\, m/s$, one can multiply the values in Figure 5 by a ratio of the desired β relative to $100\, m/s$ (or add the ratio on logarithm scale). This will produce the estimates of strain in the area covered by Figure 5.

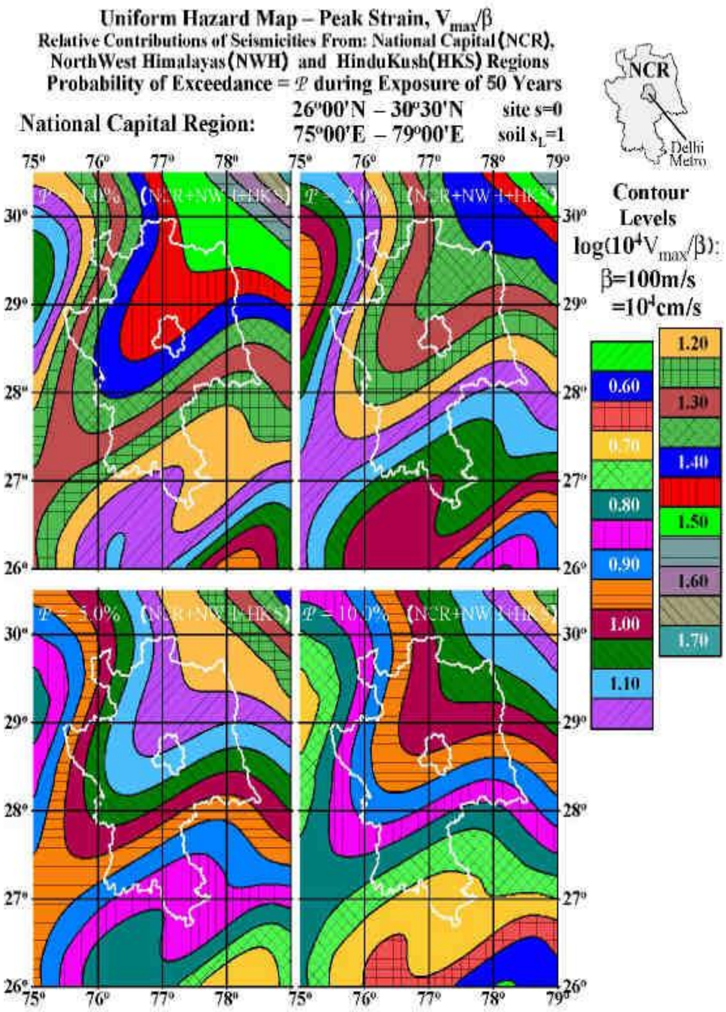

Fig. 5 Seismic Hazard map in NCR showing contours of peak strain V_{max}/β on logarithmic scale, for $\beta =$ 100 m/s, exposure period $Y = 50$ yrs, probabilities of exceedance $P = 1\%, 2\%, 5\%$ and 10%, for sites on sediments (s=0) and stiff soil (s_L=1)

For the range of probabilities of at least one exceedance between 1% and 10% during exposure of 50 years, on sediments $(s = 0)$ and on stiff soil $(s_L = 1,\ \beta = 100\, m/s)$ the peak strains range from $10^{-2.5}$ at NE to $10^{-2.8}$ at S, for P = 1% and $10^{-2.95}$ at NE to $10^{-3.6}$ at S for P = 10%, where NE and S refer to areas northeast and south of NCR.

In general, parameter β varies rapidly from site to site, so that for the site of a particular engineering project it will be necessary to estimate β by local site investigations. For a subway line, for example, measurements of β at suitably selected points along the line and then dividing $V_{\max}$ by the measured values of β will produce the desired design values for estimated surface strains probabilistically.

Empirical Criteria for Damage in Buildings Caused by Ground Shaking

A simple criterion for forecasting the expected damage to buildings due to strong ground motion is given by Duvall and Fogelson (1962) and Gupta et al. (2003) in terms of the peak ground velocity $V_{\max}$. The damage to building begins when $V_{\max}$ exceeds 5 cm/s. This can be used as a rough predictor for demarcating the areas susceptible to damage during future earthquakes.

Figure 3a, shows the range of $V_{\max}$ for probability of at least one exceedance in the range from 1% to 10%, during exposure of Y=50 yrs, at sites on sediments (s = 0) and on stiff soil (s_L = 1). Table 1 shows the corresponding range of $V_{\max}$, which are largest in north-eastern (NE) parts of NCR due to proximity to NWH seismicity, and smallest in the southern (S) parts of NCR.

Table 1: Range of peak velocities, $V_{\max}$ in cm/s for exposure during Y = 50 yrs, $s =$ 0, 1 or 2 and s_L = 1, showing the range of values between NE / S regions in NCR

P	s =0	s = 1	s = 2
1%	32 / 16	32 / 16	28 / 13
2%	25 / 10	22 / 10	20 / 10
5%	16 / 7	16 / 6	14 / 6
10%	13 / 5	11 / 4	10 / 4

The characteristics of ground motion, which contribute to the damage, includes frequency of motion, duration of motion, the type of dominant waves and distance to the source of waves, not just the amplitude of $V_{\max}$. Those contributing factors are averaged out by one-parameter approximation in the Duval and Fogelson (1962) approach. The threshold of damage also depends on the geological and soil site properties. How it varies from soft sites (e.g. sand and clay; 3 cm/s) to hard sites (e.g. sandstone, granite; 10 cm/s) has been described in Langefors and Kihlström (1978). As it is seen from Table 1, for P < 10% of at least one exceedance, all areas in NCR may experience some damaging strong ground motion during 50 years of exposure.

Differential Ground Motion

When the dimensions of the plan of a structure become large (buildings with large plan dimensions, bridges, tunnels, pipelines etc), the classical assumption that the same ground motion can be used at all the points where structure is attached to the ground ceases to be valid. In those cases, it must be assumed that the ground motion varies at the contact points with the structure and the response analysis must consider the spatial variations of ground motion.

The in-plane response of a long structure was studied by Trifunac and Todorovska (1997), while the out-of-plane response was analyzed by Trifunac and Gičev (2006). In both the cases, the spectral displacement of columns, SDC in cm, for analysis of the forces in columns due to simultaneous action of inertial forces (based on the classical SD spectrum) and pseudo static forces can be approximated by

$$SDC(T) \approx \left\{ SD^2 + f\left(V_{\max}\tau\right)^2 \right\}^{1/2}$$

where $SDC(T)$ is the relative displacement spectrum in cm/s to be used in the design of columns supporting the long structure, $V_{\max}$ is the peak ground velocity and τ is approximately the time required for the waves to travel from one end of the structure to the other. The factor f = 1 for in-plane deformation of columns (Trifunac and Todorovska (1997) while f = 2 for the out-of-plane response of columns (Trifunac and Gičev 2006).

We illustrate $SDC(T)$ for the site of the Bridge on Yamuna River (Appendix I), which is just outside the southwestern boundaries of NCR (Figure 2). It is seen from Figure 6 that the governing contribution to the $SDC(T)$ spectra is from NCR. For shorter periods $T < 0.5$ s, the increase in $SDC(T)$ amplitudes due to seismicity in NWH and HKST is very small to negligible. For longer periods $T > 0.7$ s, earthquakes in HKS source contribute more than the sources in NCR and NWH combined. This is because the Mathura bridge is near the southern end of NCR, the region with relatively small local seismicity, and also further south relative to NCR and contributions from NWH. Under those conditions the large distant earthquakes may contribute significantly to local hazard from strong ground motion, from the HKS sources in this example.

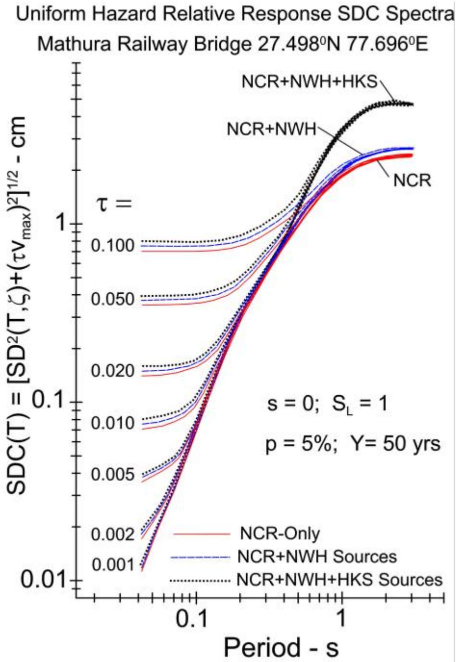

Fig. 6 Uniform hazard SDC spectrum for the site of Railway Bridge across Yamuna River (Figure 2)

The assumption in the above equation for $SDC(T)$ is that the strain in the soil between adjacent columns can be approximated by a constant. The individual spans of the Railway Bridge in Mathura (Appendix I) are all 45.7 m. From the global database on average shear wave velocity in top 30 m of ground based on topographic slope method (Allen and Wald, 2007), average shear wave velocity at the bridge site is found to be 350 m/s. This would result in $\tau \sim 0.13$ and SDC ~ 1 cm.

It is noted that most code provisions for design parameters intended to prevent unseating of bridge supports ignore the role of differential strong ground motion. This can easily be corrected by increasing the allowable sliding at supports by asymptotic values of SDC spectra as $T \rightarrow 0$.

CONCLUSIONS

We have presented seismic hazard maps for peak amplitudes of strong earthquake ground velocity, $V_{\max}$, in the National Capital Region (NCR) of India. The values of the peak velocities there depend on contributions from three contributing seismic source areas: NCR, NWH and HKS. Of those NCR and NWH contribute the most.

We have given three examples of using the hazard maps of $V_{\max}$ (a) for mapping the areas where future damage to structures may be expected, (b) how the hazard maps for $V_{\max}$ can be converted to show hazard for peak strain in the ground during passage of seismic waves, and (c) how the classical response spectra can be extended to include the differential action of earthquake ground motion on structures with long plan dimensions.

APPENDIX I – Rail Bridge Over River Yamuna at Mathura

The single-line rail bridge (No. 554) across River Yamuna in Mathura, Uttar Pradesh is located near the latitude 27.498°N and longitude 77.696°E. This bridge has 7 spans of 45.7 m each. The structural system in every span is an (simply-supported) open web girder system.

Fig. I1 Railway Bridge over River Yamuna at Mathura

The bridge is located between the Mathura and Raya stations in the Kasganj–Mathura section of North-Eastern Railway. The construction of this bridge was completed in 1885. The metre-gauge girders of the bridge were replaced in 1960. These girders were retained during the gauge conversion (to broad gauge) work that involved the strengthening/re-spacing of the stringers and other members in 2009. The bridge foundations are made of stone masonry and consist of twin wells of 4.27 m diameter and 21 m depth.

REFERENCES

1. Allen, T.I. and D.J. Wald (2007). "Topographic Slope as a Proxy for Global Seismic Site Conditions (V_S^{30}) and Amplification Around the Globe", U.S. *Geological Survey Open-File Report No. 2007-1357*, pp. 69.
2. Duvall, W.I., and Fogelson, D.E. (1962). "Review of Criteria for Estimating Damage to Residences from Blasting Vibrations", *U.S. Dept. of the Interior, Bureau of Mines, Report of Investigations No. 5968*.
3. Gupta, I.D. (2007). "Probabilistic Seismic Hazard Analysis Method for Mapping of Various Parameters to Estimate the Earthquake Effects on Manmade Structures", *Indian Society of Earthquake Technology Journal*, Vol. 44, No. 1, pp. 127–167.
4. Gupta, I.D., Tripathy, G.R. and Shirke, R.R. (2003). "Controlled Blasting for Rock Excavation in Civil Engineering Applications", *Government of India ministry of water resources, Technical Memorandum, Central Water and Power Research Station,* Khadakwasla, Pune, India.
5. Gupta, I.D. and Trifunac, M.D. (2017). "Scaling of Fourier Spectra of Strong Earthquake Ground Motion in Western Himalaya and Northeastern India", *Soil Dynamics and Earthquake Engineering,* Vol. 106, pp. 137-159.
6. Gupta, I.D. and Trifunac, M.D. (2018a). "Empirical Scaling Relations for Pseudo Relative Velocity Spectra in Western Himalaya and Northeast India", *Soil Dynamics and Earthquake Engineering,* Vol. 106, pp. 70-89.
7. Gupta, I.D. and Trifunac, M.D. (2018b). "Attenuation of Strong Earthquake Ground Motion – II: Dependence on Geology Along the Wave Paths from the Burmese Subduction Zone to Northeastern India", *Soil Dynamics and Earthquake Engineering*, Vol. 112, pp. 256-276.

8. Gupta, I.D. and Trifunac, M.D. (2018c). "Attenuation of Strong Earthquake Ground Motion – I: Dependence on Geology Along the Wave Paths from the Hindu Kush Subduction Zone to Western Himalaya", *Soil Dynamics and Earthquake Engineering,* Vol. 114, pp. 127-145.
9. Gupta, I.D. and Trifunac, M.D. (2019). "Attenuation of Fourier Amplitude and Pseudo Relative Velocity Spectra Due to Local Earthquakes in the National Capital Region of India", *Soil Dynamics and Earthquake Engineering,* Vol. 116, pp. 593-611.
10. Gupta, I.D. and Trifunac, M.D. (2023). "Attenuation of the peaks of earthquake ground motion along the Himalayan orogenic belt", ISET Jour. Earthq. Tech., Paper No. 580, Vol. 60, No. 3, pp. 75-99.
11. Gupta, I.D., V.W. Lee and M.D. Trifunac (2022a). "Seismic Microzonation of Delhi Metropolitan Area. India – II: Hazard Computation and Zoning Maps", *Earthquake Engineering and Resilience,* Vol. 1, pp. 138-163.
12. Gupta, I.D., V.W. Lee and M.D. Trifunac (2022b). "Seismic Zoning Maps of the National Capital Region (NCR) of India", *Earthquake Engineering and Resilience,* Vol. 1, pp. 268-301.
13. Langefors, U. and Kihlström, B. (1978). "Modern Technique for Rock Blasting", *J. Wiley, New Jersey, U.S.*
14. Lee, V.W. and M.D. Trifunac (2018). "Seismic Hazard Maps in Serbia", *Soil Dynamics and Earthquake Engineering,* Vol. 115, pp. 917-932.
15. Lee, V.W., Gupta, I.D., and M.D. Trifunac (2023). "Seismic Hazard Mapping for Peak Ground Velocity – I: Microzonation of New Delhi, India", ISET Jour. Earthq. Tech., Paper No. 582, Vol. 60, No. 4, pp. 113-126.
16. Todorovska, M.I. and Trifunac, M.D. (1996a). "A Seismic Hazard Model for Peak Strains in Soils During Strong Earthquake Shaking", *Earthquake Engineering and Engineering Vibration,* Vol. 16, Supplement, pp. 1-12.
17. Todorovska, M.I. and Trifunac, M.D. (1996b). "Hazard Mapping of Normalized Peak Strain in Soil During Earthquakes - Microzonation of a Metropolitan Area", *Soil Dynamics and Earthquake Eng.,* Vol. 15, No. 5, pp. 321-329.
18. Trifunac, M.D. (2016). "Site Conditions and Earthquake Ground Motion – A Review", *Soil Dynamics and Earthquake Engineering*, Vol. 90, pp. 88-100.
19. Trifunac, M.D. and A.G. Brady (1975). "On the Correlation of Seismic Intensity Scales with the Peaks of Recording Strong Ground Motion", *Bulletin of the Seismological Society of America*, Vol. 65, No. 1, pp. 139-162.
20. Trifunac, M.D. and Gičev, V. (2006). "Response Spectra for Differential Motion of Columns, Paper II: Out-of-Plane Response", *Soil Dynamics and Earthquake Engineering,* Vol. 26, No. 12, pp. 1149-1160.
21. Trifunac, M.D., & Todorovska, M.I. (1997). "Response Spectra and Differential Motion of Columns", *Earthquake Eng. and Structural Dyn.*, Vol. 26, No. 2, pp. 251-268.